Earth and Planetary Science Letters 449 (2016) 407–417

Contents lists available at ScienceDirect

Earth and Planetary Science Letters

www.elsevier.com/locate/epsl

Empirical links between trace metal cycling and marine microbial ecology during a large perturbation to Earth's carbon cycle

Jeremy D. Owens [a,b,*], Christopher T. Reinhard [b,c], Megan Rohrssen [b,1], Gordon D. Love [b], Timothy W. Lyons [b]

[a] Department of Earth, Ocean and Atmospheric Science, Florida State University, Tallahassee, FL 32306, USA
[b] Department of Earth Sciences, University of California, Riverside, CA 92521, USA
[c] School of Earth and Atmospheric Sciences, Georgia Institute of Technology, Atlanta, GA 30332, USA

ARTICLE INFO

Article history:
Received 22 October 2015
Received in revised form 25 May 2016
Accepted 26 May 2016
Available online 16 June 2016
Editor: D. Vance

Keywords:
oceanic anoxic event (OAE2)
trace metal drawdown
geochemistry
anoxia
euxinia
biomarkers

ABSTRACT

Understanding the global redox state of the oceans and its cause-and-effect relationship with periods of widespread organic-carbon deposition is vital to interpretations of Earth's climatic and biotic feedbacks during periods of expanded oceanic oxygen deficiency. Here, we present a compilation of new and published data from an organic-rich locality within the proto-North Atlantic Ocean during the Cenomanian–Turonian boundary event that shows a dramatic drawdown of redox-sensitive trace elements. Iron geochemistry independently suggests euxinic deposition (i.e., anoxic and sulfidic bottom waters) for the entire section, thus confirming its potential as an archive of global marine metal inventories. In particular, depleted molybdenum (Mo) and vanadium (V) concentrations effectively record the global expansion of euxinic and oxygen-deficient but non-sulfidic waters, respectively. The V drawdown precedes the OAE, fingerprinting an expansion of oxygen deficiency prior to an expansion of euxinia. Molybdenum drawdown, in contrast, is delayed with respect to V and coincides with the onset of OAE2. Parallel lipid biomarker analyses provide evidence for significant and progressive reorganization of marine microbial ecology during the OAE in this region of the proto-North Atlantic, with the smallest relative eukaryotic contributions to total primary production occurring during metal-depleted intervals. This relationship may be related to decreasing supplies of enzymatically important trace elements. Similarly, box modeling suggests that oceanic drawdown of Mo may have approached levels capable of affecting marine nitrogen fixation. Predictions of possible nitrogen stress on eukaryotic production, locally and globally, are consistent with the low observed levels of Mo and a rise in 2-methylhopane index values during the peak of the OAE. At the same time, the environmental challenge presented by low dissolved oxygen and euxinia coincides with increased turnover rates of radiolarian clades, calcareous nanofossils, and foraminifera, suggesting that the temporal patterns of anoxia/euxinia and associated nutrient limitation may have contributed to the fabric of OAE2-related turnover.

1. Introduction

The oceanic anoxic event at the Cenomanian–Turonian boundary (OAE2, 93.9 Ma) is one of the best documented episodes of widespread carbon burial in Earth history and is characterized by a large coeval positive carbon isotope excursion (as reviewed in Jenkyns, 2010). Despite the presence of a well-oxygenated atmosphere (Berner et al., 2003), multiple geochemical proxies record anoxic and/or euxinic (anoxic and sulfidic water column) conditions during OAE2 (Hetzel et al., 2011; Jenkyns, 2010, and references therein; Lu et al., 2010; Owens et al., 2012; Turgeon and Brumsack, 2006). During this short-lived event [~0.5 million yrs, Myr, Voigt et al., 2008, and references therein] dissolved hydrogen sulfide appears, on occasion, to have penetrated the photic zone (as reviewed in Jenkyns, 2010). However, despite the apparent extremes in oxygen deficiency, accompanied by widespread deposition of organic-rich shales, direct geochemical evidence for local bottom-water anoxia/euxinia has mostly been restricted to the Atlantic and Tethys Oceans, while redox conditions in the Pacific, Indian and Arctic Oceans remain less well constrained due to minimal geochemical analysis. Despite recent model estimates of ~40–50% ocean anoxia by volume (Monteiro et al., 2012), and

* Corresponding author.
E-mail address: jdowens@fsu.edu (J.D. Owens).
[1] Now at Department of Earth and Atmospheric Sciences, Central Michigan University, Mount Pleasant, MI 48859, USA.

http://dx.doi.org/10.1016/j.epsl.2016.05.046
0012-821X/

sulfur isotope systematics suggesting that ~5% of the seafloor was overlain by euxinic waters (Owens et al., 2013), further geochemical constraints are needed that more specifically delineate the redox structure of the wider ocean and its potential role in regulating nutrient availability. OAE2 marks a biotic turnover in the Mesozoic (Bambach, 2006, and references therein), which has been causally linked to an expansion of anoxia and/or euxinia (Leckie et al., 2002).

Increased organic carbon burial during an OAE can, in principle, be attributed to enhanced productivity and/or increased preservation (as reviewed in Jenkyns, 2010). However, maintenance of enhanced productivity and export at a global scale would require exceptional availability of major nutrients and bio-essential trace metals within the ocean. Mechanisms of enhanced nutrient delivery and/or recycling include increased hydrothermal activity (as reviewed in Jenkyns, 2010), continental weathering (Pogge von Strandmann et al., 2013, and references therein) and recycling of phosphorus from sediments due to more pervasive anoxia (Kraal et al., 2010); however, the relative contribution of each remains poorly constrained. Additionally, trace metals are important micronutrients for a range of catalytic metabolisms such as nitrogen fixation (Bellenger et al., 2011; Glass et al., 2010, and references therein), and it has been shown that growth status and nitrogen fixation rates undergo sharp changes at Mo concentrations below ~10 nM (Glass et al., 2010; Zerkle et al., 2006). In this light, we combine new and existing trace element data (Hetzel et al., 2009; Owens et al., 2012), geochemical modeling and lipid biomarkers to explore the spatiotemporal distribution of bioessential trace metals during and proximal to OAE2, with the specific goal of providing novel insight into the extent and timing of ocean redox changes and their possible impact on marine ecosystems.

2. Background

2.1. Trace metal geochemistry

The relationship between sedimentary metal enrichment, local redox and dissolved seawater concentrations is well known for modern euxinic basins (Lyons et al., 2009). For example, concentrations of Mo, V and Zn are significantly greater than those observed in oxic environments, and their relative stratigraphic variability can be explained by differences in their redox behavior. Molybdenum is the most abundant transition metal in the well-oxygenated modern ocean due to its high solubility as MoO_4^{2-} [~104 nM, Miller et al., 2011, and references therein] and is characterized by a relatively long residence time [~450 kyr Miller et al., 2011, and references therein]. Scavenging of Mo by Mn-oxide phases is an important removal pathway in the ocean; however, Mo is most efficiently buried in the presence of free sulfide, both in the sediments and the water column, with the latter being substantially more effective (Scott and Lyons, 2012). We distinguish between sulfidic sediments and a sulfidic water column and define *reducing environments* as those in which sulfide accumulation is restricted to pore fluids. These conditions often occur beneath low-oxygen bottom-waters similar to modern oxygen minimum zone environments (Little et al., 2015). In the modern oxic ocean, V is characterized by a shorter residence time [~50 to 100 kyr, Algeo, 2004; Morford and Emerson, 1999] and a smaller dissolved marine reservoir [35 to 45 nM, Morford and Emerson, 1999, and references therein], regulated primarily through its removal as vanadate oxyanions (HVO_4^{2-} and HVO_4^-) associated with Mn- and Fe-oxides and by efficient burial in low oxygen settings (as reviewed by Tribovillard et al., 2006).

Efficient sequestration of sedimentary V starts in low oxygen environments and continues through euxinic conditions (Algeo, 2004; Morford and Emerson, 1999). Therefore, in contrast to Mo, reductive enrichment of V in marine sediments can be independent of sulfide. We can therefore use V as an indicator of low oxygen and anoxic conditions—an important contrast to the sulfide-dependent enrichment of Mo. The residence time of Zn is also relatively short, ~11 ka (Little et al., 2014), with a small dissolved marine concentration of ~5.4 nM. Importantly, sequestration of sedimentary Zn, like V, begins in low oxygen environments and continues through euxinic conditions (Algeo, 2004). Under low oxygen conditions both V and Zn are likely associated with organic matter, humic and fulvic acids and are buried as vanadyl ion and sphalerite minerals, respectively (Algeo, 2004; Tribovillard et al., 2006).

2.2. Organic geochemistry

In thermally immature, sulfur-rich sedimentary rocks, a high proportion of the total biomarker pool is often bound covalently in geomacromolecules due to early diagenetic vulcanization processes that take place in euxinic water columns and shallow sediments (Sinninghe Damsté and de Leeuw, 1990). Selective preservation of lipids in these environments may lead to signal bias in biomarker records (Kohnen et al., 1992; Sinninghe Damsté and de Leeuw, 1990) if only the extractable (free) hydrocarbons are analyzed. Catalytic hydropyrolysis (HyPy) is a well-established analytical technique for generating high yields of hydrocarbon products from kerogen and immature sediment while retaining important structural and stereochemical features (Love et al., 1995). HyPy has been useful in previous studies of OAE samples (Blumenberg and Wiese, 2012).

Hopanoids and steroids are polycyclic lipids that are synthesized by diverse groups of bacteria and eukaryotes, respectively, with similarly high preservation potential in the geological record. The Phanerozoic marine average for the hopane/sterane ratio for organic-rich rocks and oils typically lies in the range of 0.5–2.0 (Cao et al., 2009). Additionally, abundance patterns for the steroid carbon number in the C_{27}–C_{30} range broadly reflect the algal community composition (e.g., Kodner et al., 2008; Schwark and Empt, 2006; Volkman, 2003). C_{29} steroids are the precursors to the 24-ethylcholestanes found in ancient rocks and oils and are particularly abundant in green algal clades, whereas C_{27} sterane (cholestane) precursor lipids are more abundant in red algae (rhodophytes and dinoflagellates) (Kodner et al., 2008). C_{28} steroids (preserved as 24-methylcholestanes) are important in higher order endosymbiotic red algal lineages that were not dominant or diverse until late Mesozoic time and younger (Grantham and Wakefield, 1988), including haptophytes and diatoms, but also in some prasinophytes from the green lineage (Kodner et al., 2008; Volkman, 2003). The C_{30} steranes, 24-*n*-propylcholestanes are mainly derived from sterol precursors produced by the exclusively marine algal class Pelagophyceae, although these have also been reported as minor constituents of foraminifera (Giner et al., 2009; Grabenstatter et al., 2013).

3. Materials and methods

3.1. Samples

We present a compiled organic and inorganic dataset from a high-resolution spliced section from Demerara Rise, Ocean Drilling Program (ODP) Site 1258, holes 1258A, 1258B and 1258C (Fig. 1). Site 1258 was the deepest of the holes drilled during Leg 207, estimated to have been at paleodepths >1000 m. The Demerara Rise transect of Leg 207 was along the continental slope, approximately hundreds of kilometers from the coastline of Suriname (Erbacher et al., 2004). Importantly, past researchers have argued that connections between this region and the open proto-North Atlantic

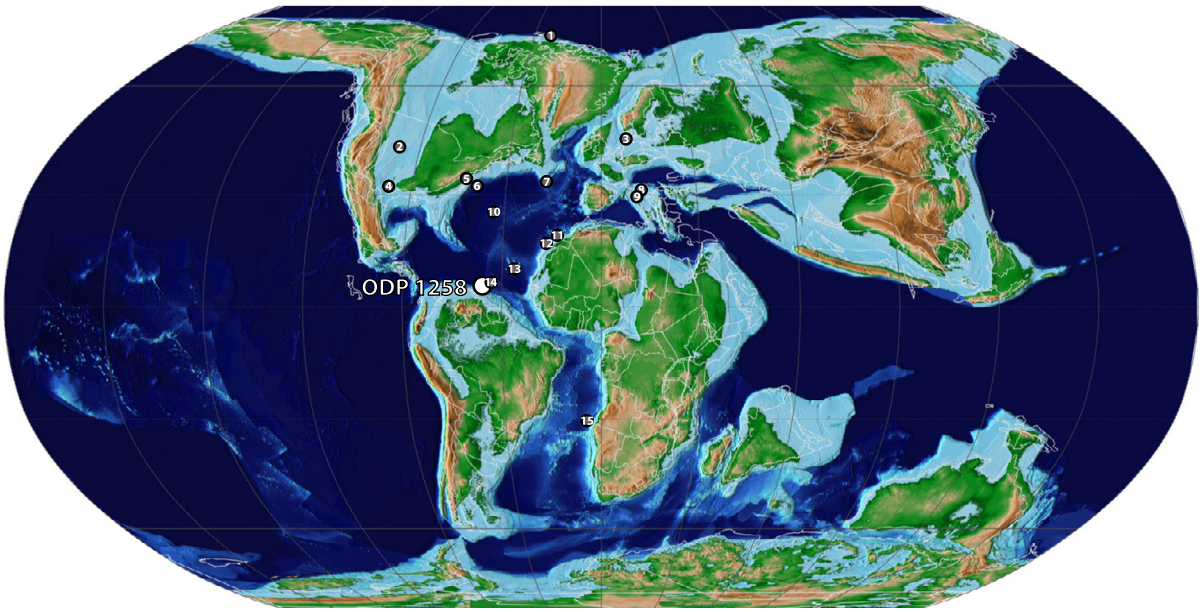

Fig. 1. Paleogeographical reconstruction with ODP 1258 highlighted in white. Additional markers indicate sites with published Mo and TOC values during OAE2 (see Table 1). The dark blue indicates deep sea settings, the light blue represents shallow-marine settings, and green and brown designate the continental land masses for 94 Ma (Scotese, 2008). Numbers for additional sample localities are referred to in Table 1.

were not restricted (Erbacher et al., 2004; MacLeod et al., 2008 and references therein). Meter composite depth (mcd) below seafloor for holes 1258B and 1258C for the new data presented here were adjusted based on correlation with the carbon isotope stratigraphy of hole 1258A. This approach was adopted by Erbacher et al. (2005) and subsequently used in additional publications (Hetzel et al., 2009; MacLeod et al., 2008; Owens et al., 2012). This composite section is characterized by a nearly continuous record of finely laminated, organic-rich sedimentary deposition preceding, during and subsequent to the OAE—a unique feature among sites that record OAE2.

3.2. Methods

Prior to analysis, all samples were examined for signs of oxidation, such as elemental sulfur and other secondary sulfur compounds from pyrite oxidation, along with related iron oxide coatings on the core surfaces. Oxidized surfaces were then removed using a saw prior to further processing. Samples were then crushed and homogenized using a ceramic trace metal-clean ball mill. See appendix for more detail on all methods.

3.2.1. Carbon

Determination of new data for total inorganic carbon (TIC) via acidification and total carbon (TC) via combustion was performed on an Eltra CS-500 carbon–sulfur analyzer. Total organic carbon (TOC) is calculated by difference (TOC = TC − TIC).

3.2.2. Fe geochemistry

Briefly, distinct Fe species were isolated by a series of sequential chemical extractions (Poulton and Canfield, 2005). First, carbonate-associated iron (Fe_{carb}) was extracted using a sodium acetate solution, followed by a sodium dithionite solution to dissolve oxide-bound iron (Fe_{ox}). During the final step, magnetite iron (Fe_{mag}) was extracted using an ammonium oxalate/oxalic acid solution. Iron in the three solutions was analyzed via inductively-coupled-plasma mass-spectrometry (ICP-MS) using an Agilent 7500ce. Replicate analyses are reproducible within 7%. Highly reactive iron (Fe_{HR}) was calculated by summing Fe_{pyrite} (Fe_{py}), Fe_{carb}, Fe_{ox} and Fe_{mag}. Concentrations of Fe_{py} were estimated from the pyrite sulfur content—as measured through conventional chromium reduction analysis followed by iodometric titration (Canfield et al., 1986)—assuming a stoichiometry of FeS_2.

3.2.3. Elemental concentration

Elemental concentrations were initiated via a standard sequential acid digestion and quantified using an ICP-MS. In all cases, analyses of standard reference materials (SDO-1 shale) were within the accepted analytical error for all pertinent elements. Specifically, iron yielded errors less than ±4%, and Mo, V and Zn had errors less than ±6%. Procedural blanks were below detection limits.

3.2.4. Organic analysis

Powdered samples were extracted in a Microwave Accelerated Reaction System (CEM Corp.) with dichloromethane and methanol (9:1 v/v) at 100 °C for 15 min. Extracted sediment residues were impregnated with ammonium dioxydithiomolybdate [$(NH_4)_2MoO_2S_2$], which decomposes during hydropyrolysis (HyPy) conditions above 250 °C. HyPy was conducted using a continuous flow catalytic hydropyrolysis apparatus as described by Love et al. (1995). Solvent extracts and hydropyrolysates were separated into aliphatic, aromatic and polar fractions by silica gel column chromatography. Gas-chromatography mass-spectrometry (GC-MS) analyses of saturated and aromatic hydrocarbons were conducted in full scan mode over a mass range of 50 to 600 Da. These analyses were accomplished using an Agilent 5973 MSD mass spectrometer interfaced to an Agilent 7890A equipped with a DB-1MS capillary column (60 m × 0.32 mm, 0.25 μm film) and run with He as carrier gas. Hopanoid/steroid ratios were calculated as the sum of free hydrocarbon (solvent extracts) plus kerogen-bound (HyPy) C_{27}–C_{35} hopanes/enes (m/z 191) divided by the sum of free hydrocarbon plus kerogen-bound C_{27}–C_{29} steranes (m/z 217) and sterenes (m/z 215).

We used Metastable Reaction Monitoring-Gas Chromatography-Mass Spectrometry (MRM-GC-MS) for monitoring the relative abundance of dinosteranes (4,23,24-trimethylcholestanes) and 4-methyl-24-ethylcholestanes to regular steranes (4-desmethyl steranes) to assess source contributions from dinoflagellates to the eukaryotic planktic community and for calculating 2-Methylhopane Indices (2-MeHI). These analyses were performed using a Waters

Autospec Premier mass spectrometer equipped with an Agilent 7890A gas chromatograph and DB-1MS coated capillary column (60 m × 0.25 mm, 0.25 μm film) using He for the carrier gas. Procedural blanks were analyzed to ensure very low levels of background biomarker compounds for both extractions and hydropyrolysis products.

3.2.5. Modeling

We employ a variant of the mass balance model developed in Reinhard et al. (2013), in which oceanic Mo is treated as a single well-mixed reservoir. The size of the Mo reservoir is controlled by the balance between a primary input flux—predominantly riverine input through continental weathering of sulfides and organic matter hosted in exposed crustal materials (Miller et al., 2011)—and a series of permanent removal fluxes from the marine reservoir associated with the burial rate in oxic sediments (α_{ox}), reducing sediments (α_{red}) and sulfidic environments (α_{sulf}). The general equation for the globally averaged seawater concentration of Mo is given as:

$$\frac{d}{dt}M_{\mathrm{Mo}}^{sw} = J_{in} - \sum_{i} A_i b_i^{ini} R_{\mathrm{Mo}}^{\alpha_i},$$

where M_{Mo}^{sw} is the seawater reservoir mass of dissolved Mo. Parameters A_i, b_i^{ini} and $R_{\mathrm{Mo}}^{\alpha_i}$ denote the area, initial (background) burial rate and normalized seawater reservoir ($[\mathrm{Mo}]_t/[\mathrm{Mo}]_0$) for a given sink I, respectively. The term α_i represents the burial rate exponent for a given marine sink, essentially specifying the shape of the feedback relationship between marine reservoir size and the magnitude of each removal flux.

The relatively high and stable pO_2 values thought to characterize most of the Phanerozoic (Berner et al., 2003) indicate that sulfide and organic matter weathering would be largely 'transport limited', that is, limited by the rate of erosional stripping and thus exposure to the atmosphere (i.e., West et al., 2005) and are therefore unlikely to dictate perturbations to the marine reservoir over the time scales of interest in this study. As such, we consider it likely that major perturbations to the marine Mo reservoir will be most readily dictated by changes in the sink terms and thus the redox structure of the ocean.

Assuming steady state and that all burial rate exponents are similar ($\alpha_{ox} \sim \alpha_{red} \sim \alpha_{sulf}$), expansion of the sink term i allows us to solve for the initial globally averaged sulfidic burial rate (b_{sulf}^{ini}):

$$b_{sulf}^{ini} = \left[\frac{J_{in}}{R_{\mathrm{Mo}}^{\alpha}} - A_{ox} b_{ox}^{ini} - A_{red} b_{red}^{ini}\right] A_{sulf}^{-1}$$

Following Reinhard et al. (2013), we specify that the burial capacity of reducing marine environments that will bury significant authigenic Mo decreases in a logarithmic fashion with increasing bathymetric depth. The result is an overall decrease in globally averaged burial capacity as large regions of the seafloor become reducing. This relationship is not particularly well-constrained, but our model is governed primarily by varying a scaling parameter (σ_{Mo}) to adjust the initial globally averaged sulfidic burial rate (b_{sulf}^{ini}) to that characteristic of the modern ocean when all other parameters are set to modern values.

4. Results

4.1. Geochemical data

A composite 10 m section from Site 1258, incorporating data from Erbacher et al. (2005), Hetzel et al. (2009), Owens et al. (2012) and new data from this study is marked by generally high organic carbon contents ranging from 0.5 to 30 wt% and carbonate contents ranging from 0 to 95 wt% (Fig. 2). Interestingly, local TOC contents, on a carbonate-free basis, show very minimal increases during the OAE, with average TOC values of 18.8 wt% for non-OAE intervals and 21.9 wt% during the OAE. Importantly, Site 1258 maintains relatively stable and elevated Fe_{HR}/Fe_T and Fe_{py}/Fe_{HR} ratios throughout the section—with averages of 0.82 ± 0.12 and 0.76 ± 0.09, respectively (Fig. 2). These values do not include Fe_{ox} due to possible post-drilling oxidation of pyrite (see Discussion).

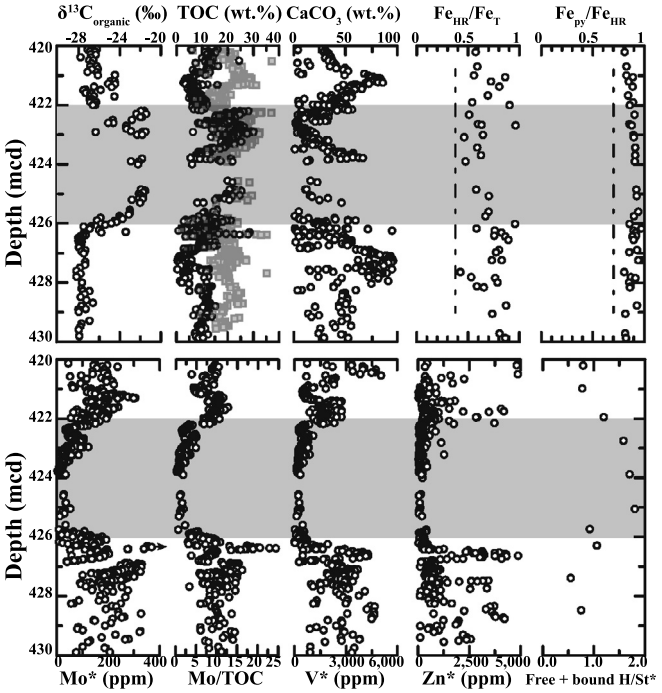

Fig. 2. Stratigraphic trends for inorganic and organic trends where OAE2 is marked by the gray box, delineated by the positive carbon isotope excursion. The ∗ denotes that these plots are corrected for carbonate content. There are four data points for Mo∗ that are not plotted, and that are above the axis maximum (426.35 to 426.37 mcd) with values up to 796 ppm. H/St^ is the hopanoid/steroid ratio calculated from quantitative lipid biomarker analysis for the combined (free hydrocarbon + kerogen-bound) biomarker pools and is a broad measure of the balance of bacterial/eukaryotic source organism inputs. The gray squares in the TOC panel represent are carbonate corrected values for TOC showing that the variation in TOC is partially due varying amounts of carbonate. The $\delta^{13}C$ data is from Erbacher et al. (2005), elemental concentrations/ratios and TOC and trace metals are from Hetzel et al. (2009), Owens et al. (2012) and this study.

The magnitude of trace metal enrichments can be influenced by carbonate dilution, but our observed trends are not a product of this potential artifact. Specifically, the data plotted on a carbonate-free basis (Fig. 2) show trends that are very similar to those for the non-normalized data (all data in appendix). More to the point, the carbonate contents during the OAE (Fig. 2) are low compared to those before and after. As a result, the systematic differences in trends for Mo, V and Zn during the event compared to the data from before and after are actually muted by the greater impact of pre- and post-event carbonate dilution. The non-OAE average baseline for carbonate-free Mo at this locality is 184 ± 91 ppm (all ranges are 1 standard deviation of the data), while the average carbonate-free Mo concentration during the OAE drops to 56 ± 38 ppm. The carbonate-free V and Zn concentrations outside the OAE are $2,151 \pm 1,134$ and $1,258 \pm 1,798$ ppm, respectively, while carbonate-free concentrations drop to an average of 522 ± 384 and 211 ± 321 ppm, respectively, during OAE2. The non-OAE V and Zn include decreasing values observed just prior to the OAE (see Discussion). Furthermore, a ~3-m mid-portion of the OAE [422.99 to 425.92 mcd] preserves very low enrichments of all three elements. At the nadir of the event, defined by the

plateau of the $\delta^{13}C$ curve, Mo, V and Zn enrichments approach the crustal averages of ~2 ppm, ~180 ppm and ~75 ppm (Taylor and McLennan, 1995), respectively—with observed respective average concentrations of 18 ± 10, 263 ± 79 and 110 ± 89 ppm, including Mo concentrations as low as ~2 ppm.

4.2. Lipid biomarker stratigraphic trends

We analyzed the stratigraphic distributions and abundances of hopanes plus hopenes (C_{27}–C_{35}) and steranes plus sterenes (C_{27}–C_{30}) in ten kerogen hydropyrolysates and corresponding solvent extracts to assess the relative sedimentary contributions of bacteria and eukaryotes. Solvent extractable hydrocarbons yielded results comparable to previous lipid biomarker results reported for sediments from Site 1258 (Forster et al., 2004). The sample coverage was chosen to capture the biomarker record pre-, syn- and post-OAE, coincident with the trace metal trends. Table S1 indicates that, as expected for low maturity, high sulfur sediments, >85% of the total hopanoid and steroid biomarkers considered here were generated from the kerogen via cleaving of covalent-linkages. Product profiles and the consistency of the thermal maturity relationships between free and bound portions of the biomarker pool argue for a predominantly autochthonous marine origin for both free and bound biomarkers at Site 1258.

The observed stratigraphic trends for hopanoid/steroid (H/St) ratios are similar to previous results from the end-Permian (Cao et al., 2009), with the highest ratios observed during the positive C_{org} excursion. However, it has been documented that absolute values for H/St for free hydrocarbons and kerogen-bound pools are different due to selective biomarker partitioning in immature S_{org}-rich rocks (Kohnen et al., 1992). As such, we focus on the total (free plus bound) hopanoid/steroid ratio to get the quantitatively most accurate picture of the magnitude of change in this ratio observed through OAE2 at Site 1258. Major shifts in hopanoid/steroid ratios largely record changes in the balance of bacterial versus algal primary production. An approximately two- to three-fold increase in the total H/St biomarker ratio is observed [pre-OAE average of 0.79 ($n = 3$); OAE average of 1.50 ($n = 4$) and maximum of 1.80; and a post-OAE average of 0.92 ($n = 3$); see Fig. 2 and Table S1].

Steranes are typically much more abundant in the hydropyrolysis products than extracts; therefore, we focus on carbon number distributions in the bound pool. Free and bound sterenes and free and bound steranes all have very similar stratigraphic trends. Prior to the onset of the OAE, C_{28} and C_{27} steranes are similarly abundant (average 32 and 33% of total C_{27} to C_{30} steranes, respectively, $n = 3$), with C_{29} steranes somewhat less common at 27%. C_{30} regular and 4-methylsteranes are much less abundant at 5 and 2%, respectively. During the OAE ($n = 4$), the relative abundance of C_{28} steranes drops to 25%, while C_{29} steranes increase to 30%, and, most significantly, C_{27} steranes become most abundant at ~38% of the total C_{27}–C_{30} steranes. C_{30} steranes decrease to 3%, and 4-methylsteranes from dinoflagellates increase to 4% during the OAE. Thus, during the peak of the OAE, the sterane carbon number patterns suggest that red algal classes that produce C_{27} compounds as their major membrane sterols became more abundant within the eukaryotic planktonic community. After the OAE ($n = 3$), distributions return to values similar to pre-OAE profiles, with C_{27} and C_{28} again most abundant at 34 and 33%. C_{29} steranes are less abundant at 27%. C_{30} steranes increase slightly up to 4%, while 4-methylsteranes decline to 3%.

4.3. Modeling

Our steady-state model can produce a significant Mo drawdown due to an expansion of global euxinic conditions (Fig. 3). We vary σ_{Mo} and α_{sulf} values over a relatively wide range and solve the model at steady state for a globally averaged seawater [Mo] value of 10 nM, the biological nitrogen fixation threshold (Glass et al., 2010; Zerkle et al., 2006). These results show that there are large regions of free parameter space that produce globally averaged seawater [Mo] at or below ~10 nM, but euxinic expansion remains at or below estimates from Owens et al. (2013). Our model, while paying careful attention to the key parameters and being among the most comprehensive attempted to date, may be oversimplified in that it assumes that the strength and interrelationship of all burial rate feedbacks are identical. Indeed, it is easy to imagine mechanistic reasons they could differ, but those additions are beyond the scope of this study. In addition, the scaling approach of the offshore burial rate of Mo used here is not inclusive of all burial rates due to the shallowness of modern euxinic basins. Nevertheless, steady-state Mo modeling suggest that obtaining ~10 nM seawater values is possible with euxinic bottom waters covering 7% or less by area of the ocean bottom, which is in good agreement with inferences from the S isotope record (Owens et al., 2013).

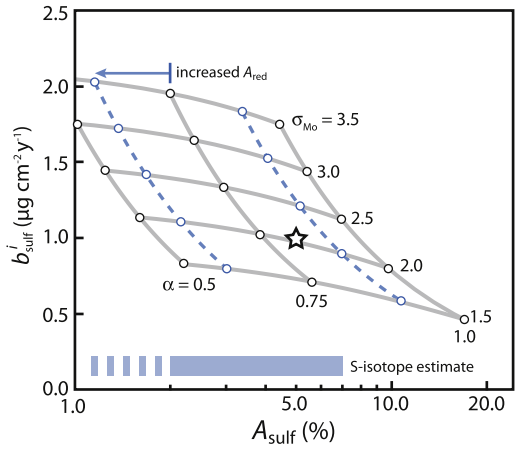

Fig. 3. Steady state analysis of Mo mass balance model discussed in the text. On the *y*-axis is the sulfidic burial rate of Mo and on the *x*-axis is the area of sulfidic bottom water. Vertical contours show isolines for [Mo] = 10 nM at a range of burial feedback coefficients (labeled according to α value) — showing, for example, that with a sulfidic seafloor area equivalent to ~5% of modern seafloor area and a globally integrated initial Mo burial rate of ~1.0 μg cm^{-2} y^{-1} (star) seawater [Mo] will only exceed ~10 nM if $\alpha > 0.75$. Vertical blue contours show the same calculations with an additional doubling of reducing seafloor area, and are meant to schematically depict the sign and magnitude of changes associated with relaxing the assumption of constant A_{red}.

5. Discussion

5.1. Drawdown of metals during the OAE and biotic response

We first explored the local depositional redox chemistry by analyzing the associated Fe geochemistry for 43 samples over the 10 m section. The sequential Fe extraction method differentiates among the highly reactive iron phases (Poulton and Canfield, 2009) that are reactive to hydrogen sulfide on the short time scales of deposition and shallow burial. Values above 0.38 for Fe_{HR}/Fe_T ratios are diagnostic of deposition under anoxic conditions. These elevated values, in combination with elevated Fe_{py}/Fe_{HR} (>0.7), suggest deposition beneath euxinic waters because nearly all of the reactive Fe has been converted to pyrite (März et al., 2008; Poulton and Canfield, 2009). Sulfide-rich (euxinic) depositional settings are, by definition, reactive Fe-limited (Raiswell and Berner, 1986). Importantly, Site 1258 maintains relatively stable and elevated Fe_{HR}/Fe_T and Fe_{py}/Fe_{HR} ratios throughout the section—consistent with local euxinia before, during and following OAE2 (Fig. 2).

Due to the considerable amount of time between drilling and Fe extraction (~10 yrs), we must consider the possibility that some if not all of the Fe_{ox} is a product of pyrite oxidation during core storage. This possibility is supported by the low amounts of Fe_{ox} in a low resolution sample set from the same core analyzed soon after collection (published three years after drilling; Böttcher et al., 2006), which could be predicted given the high amounts of organic carbon and associated expectation that any residual Fe(III) would likely be reduced by bacteria or through reaction with H_2S. Because it is likely that the samples have experienced some post-drilling pyrite oxidation, there is a risk of 'double counting' Fe_{py} in our calculation of Fe_{HR} because chromium reduction will quantify the elemental sulfur derived as an initial product of pyrite oxidation, and any Fe_{ox} resulting from pyrite oxidation will be extracted during the dithionite step. Therefore, we do not include Fe_{ox} in our calculation of Fe_{HR} as plotted in Fig. 2, although Fe_{HR} calculated with and without Fe_{ox} is presented in the Appendix. Importantly, Fe_{ox} is generally very low in our samples (ranging from 0.02 to 0.71 wt% and averaging 0.17 wt%), consistent with Böttcher et al. (2006). Furthermore, even with the inclusion of Fe_{ox} in our calculations of Fe_{HR}, most of the samples (33 of 43) would still show Fe_{py}/Fe_{HR} ratios above the euxinic threshold value of 0.7 (März et al., 2008).

Such independent constraints on local redox provide crucial context for the interpretation of trace metal enrichment records and, more specifically, are essential for assessing global controls on trace metal inventories. For example, varying magnitudes of trace metal enrichment recorded in black shales during locally persistent euxinia are reasonably attributed to time-varying changes in seafloor redox, with lower local enrichments reflecting a larger global extent of oxygen deficiency (Reinhard et al., 2013, and references therein). We note, however, that other factors (organic carbon fluxes, local sulfide levels, bulk sediment mass accumulation rates, etc.) translate into some degree of uncertainty in quantifying those global extents and are important avenues of further model development (e.g., Lyons et al., 2014). In any case, our independent environmental context indicates that Site 1258 should provide an ideal window into ocean/global-scale marine redox.

Substantial trace metal drawdown observed during OAE2 (Fig. 2) suggests a dramatic and widespread perturbation to the marine geochemical redox system that impacted global metal inventories and isotopes (Dickson et al., 2016; Goldberg et al., 2016; Hetzel et al., 2009; van Helmond et al., 2014). Again, the persistence of local euxinia throughout the analyzed interval at Site 1258 confirms that shifting *local* redox is not the primary control on the observed metal enrichment pattern, and we can think of no reasonable local inventory control that would assert itself differentially over the entire interval of interest (see below). Additionally, the observed trace metal trends are unlikely to be driven by differential incorporation into organics due to elevated organic carbon content throughout the section, although the drawdown of metals could affect porphyrin preservation (Junium et al., 2015). At the nadir of trace metal drawdown, sedimentary Mo, V and Zn enrichments (carbonate-corrected) decrease by as much as 90% at Site 1258 (e.g., average Mo concentrations decrease from 184 ppm to 18 ppm) during continuously euxinic local deposition.

Additionally, and importantly, the decline in V and Zn enrichments precedes the OAE and associated Mo depletion (based on the concentration of each element declining to near crustal values – Mo at 425.74 m and V at 426.32 m) by ~0.6 m or ~75 kyr assuming a linear sedimentation rate of ~8 m/myr—based on the estimated 0.5 myr duration of OAE and its 4 m thickness (Fig. 4). It should be noted that using a longer duration for OAE2 would increase the amount of time between the drawdown of these two elements. Once Mo drawdown begins, it is very rapid (~25 kyr)—from 140 ppm at 426.08 mcd to <50 ppm at 425.88 mcd—despite its long residence time. As such, we argue that the offset between the drawdown of V and Zn versus Mo is unlikely to have been driven by differences in the residence (response) times for the three metals. Instead, this offset is most easily explained by dramatic increases in metal uptake (V and Zn) via large-scale expansion of anoxia, followed by subsequent expansion of euxinic conditions that impacted the Mo reservoir.

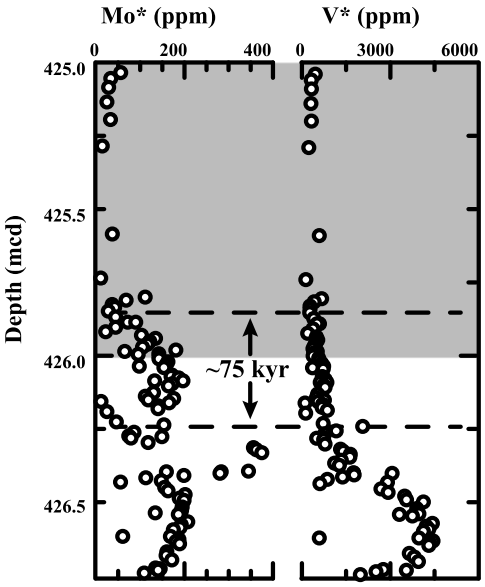

Fig. 4. An in-depth view of the stratigraphic plots from Fig. 2 for Mo and V for Site 1258 (gray box represents OAE2). Note the drawdown of V prior to the OAE while the nadir in Mo enrichment is not achieved until after the onset of the OAE. The lower dashed line indicates the initial drawdown of V and the upper line delineates the start of the muted Mo enrichments. These two horizons are separated by ~75 kyr. Similar to Fig. 2 there are 4 outliers not included on the plot for clarity.

5.2. Mo-TOC intersite comparison

There is a broad similarity between modern euxinic basins and OAE2 data from Site 1258 in terms of the observed Mo-TOC relationship (Algeo and Rowe, 2011; Hetzel et al., 2009). It is well documented in the modern ocean that Mo co-varies with TOC in euxinic settings (Algeo and Lyons, 2006; Lyons et al., 2009). Further, the modern euxinic Black Sea records low Mo/TOC values due to the relatively low bottom-water Mo concentrations (Lyons et al., 2009), while open-ocean euxinic localities such as the Cariaco Basin record greater Mo/TOC due to a more open-ocean supply of Mo (Algeo and Lyons, 2006; Lyons et al., 2009). Therefore, the Mo/TOC relationship in modern euxinic basins is highly dependent on the Mo inventory of the water column.

Site 1258 shows a similar Mo/TOC relationship with two distinct populations (Algeo and Rowe, 2011; Hetzel et al., 2009). Specifically, the non-OAE (pre- and post-OAE2) samples show ratios similar to those from the Cariaco Basin, while ratios from the OAE resemble those from the Black Sea. Importantly, similarly low Mo/TOC ratios are recorded in numerous organic-rich OAE2 localities (Table 1) from several ocean basins, including the Western Interior Seaway and the proto-North and -South Atlantic and Tethys oceans (see Fig. 1 and Table 1). Averages of the individual ratios at each location are all below 6.5 (see supplemental information for more details). Note that we do not include sites with anomalously low sedimentation rates; a lack of stratigraphic data or, obviously, samples lacking companion Mo and TOC data. The included localities show a collective, uncorrected average Mo concentration during the OAE of ~25 ppm, and the average TOC for these sections is 8.7 wt% (Table 1). We note that

Table 1
Overview of the known Mo and TOC data with independent evidence for redox conditions during the OAE. Site number refers to the label on Fig. 1.

Name	Site #	Average			*n*	Max			Independent euxinia during OAE		Reference
		Mo (ppm)	TOC (wt %)	Mo/TOC		Mo (ppm)	TOC (wt %)	Mo/TOC	Extent	Evidence	
ODP 1258	1258	44.2	17.1	2.8	217	117.0	30.2	10.4	Constant	Fe speciation	Hetzel et al. (2009), this manuscript
May Point	1	2.5	5.2	0.3	9	5.0	12.9	1.3			Lenniger et al. (2014)
Portland Core	2	1.8	1.1	2.7	27	6.0	5.2	9.1			Meyers et al. (2005)
Wunstorf	3	5.0	1.0	5.3	6				Unknown		Hetzel et al. (2011)
Iona	4	2.1	2.5	0.9	19	9.2	5.9	2.3			Eldrett et al. (2014)
DSDP 603B	5	17.7	6.6	3.5	8	65.0	11.6	9.3	Periodic	Biomarkers	Owens et al. (2012) and references therein
DSDP 105	6	18.5	11.8	1.8	18	76.6	19.5	7.4	Periodic	Biomarkers	Owens et al. (2012) and references therein
DSDP 1276	7	5.8	4.2	1.4	28	22.9	12.7	5.7	Unknown		Westermann et al. (2014)
Furlo	8	12.9	7.5	1.6	29	58.5	18.4	4.7			Turgeon and Brumsack (2006), Westermann et al. (2014)
La Contessa	9	14.9	9.8	2.0	13	47.8	20.4	4.2	Periodic	Fe speciation	Westermann et al. (2014)
DSDP 386	10	34.6	7.7	4.3	12.0	70.0	13.0	6.5	Unknown		van Helmond et al. (2014)
Tarfaya S57	11	8.2	9.0	0.8	75.0	52.3	20.0	6.2	Dominate	Fe speciation	Goldberg et al., 2016 and references therein
Tarfaya S75	12	14.7	6.2	2.2	12	49.4	11.1	7.0	Unknown		Owens et al. (2012)
ODP 367	13	107.4	24.3	5.7	18	235.3	38.6	17.0	Constant	Biomarkers	Owens et al. (2012), Westermann et al. (2014)
ODP 1260	14	36.7	12.9	3.2	24	129.0	23.1	6.9	Unknown		Hetzel et al. (2009), this manuscript
DSDP 530	15	76.0	11.6	6.5	18	215.0	19.8	10.9	Unknown		Forster et al. (2008)
Modern Black Sea		45	6.1	7.4		190	17.3	11.0			Algeo and Lyons (2006)
Modern Cariaco Basin		85	4.4	19.3		187	6.2	30.2			Algeo and Lyons (2006)

only some of these past studies have used independent analysis beyond trace metal enrichments, such as organic biomarkers or Fe speciation, to demonstrate euxinia (Kuypers et al., 2004a; Lenniger et al., 2014; Owens et al., 2012; Westermann et al., 2014). Further, some sites were thought to have been anoxic but not euxinic based on Fe speciation; however, this relationship could be due to post-depositional pyrite oxidation (Lenniger et al., 2014; Owens et al., 2012; Westermann et al., 2014). In fact, many of the localities have been interpreted as low oxygen environments, rather than euxinic, due to slightly enriched but still muted Mo enrichments—thus missing the possibility of temporally varying reservoir controls under persistently euxinic local conditions. We would expect that all redox sensitive (Mo, V, Zn, etc.) elements behave similarly, where a global reduction of the marine trace metal reservoir size would cause low enrichments of redox sensitive elements even in the face of euxinic conditions, as witnessed at Site 1258.

5.3. Modeling Mo drawdown

The observed trend in Mo concentrations suggests a dramatic perturbation to the geochemical redox evolution of the ocean during OAE2. To explore the possibility of marine seawater [Mo] drawdown we have calculated the parameter space (burial rate, α, σ_{Mo} and bottom water redox conditions) needed to maintain [Mo] at the biological threshold of ~10 nM as defined by nitrogen fixation (Glass et al., 2010; Zerkle et al., 2006). The Mo data suggest a 90% drawdown of the Mo reservoir thus reaching ~10 nM concentration if the starting value was close to modern values (107 nM). Fig. 3, shows that achieving the biologically significant threshold of 10 nM seawater Mo concentration can be accomplished with minimal euxinic conditions, as constrained by C and S isotope systematic of 3 to 7% euxinic seafloor (Owens et al., 2013). The model does not provide a unique solution as there are several under-constrained parameters (e.g., exact values for burial rate, α and σ_{Mo}).

Despite uncertainties in the specific combination of parameters, it seems clear that the marine reservoir of Mo can be diminished dramatically by a marine redox perturbation on the order of OAE2—with the implication that the seawater reservoir size of redox-sensitive trace metals can be severely impacted by benthic redox structure even under relatively high atmospheric pO_2. It is possible that marine Mo concentrations during Phanerozoic perturbations to ocean chemistry (such as OAE2) approached levels that may have impacted the overall nutrient status of some surface ocean environments. We emphasize that the globally integrated impact of such perturbations to metal micronutrient availability and the potential for biological adaptation to low nutrient levels are not well understood (see Glass et al., 2010, for discussion; Reinhard et al., 2013). That said, our analysis highlights the significant impact that transient perturbations to seawater micronutrient chemistry may have had on the entire ocean for the cycling of carbon, oxygen and trace element during the Cretaceous. We anticipate similar impacts on local pelagic ecology. This finding is corroborated by nitrogen isotope data at Site 1258 (Higgins et al., 2012; Junium et al., 2015; Zhang et al., 2014), which suggest a reduction in Mo-based nitrogenase during OAE2.

Our model calculations are performed assuming constant input fluxes, while only manipulating seafloor redox conditions (oxic, reducing and sulfidic burial); however, increases in continental weathering have also been documented during OAE2 (Pogge von Strandmann et al., 2013, and references therein). These increases could influence sedimentation rates and trace element input rates to the ocean. A significant increase in the input flux from continental weathering would require a greater extent of euxinia and/or reducing environments to produce the same Mo drawdown. How

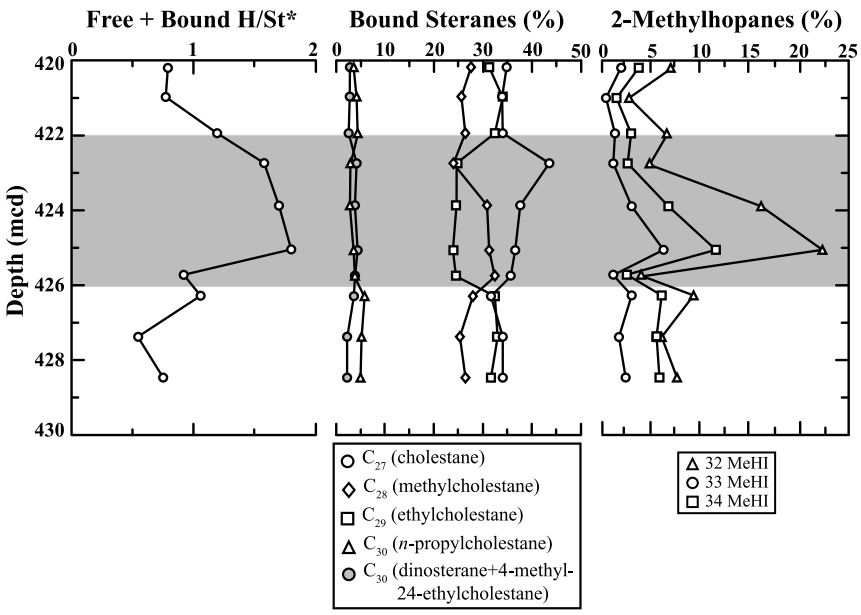

Fig. 5. Stratigraphic records of hopanoid/steroid calculated from total biomarker yields (free hydrocarbon + kerogen-bound), bound sterane carbon number patterns as percentages of total C_{27}–C_{30} steranes, and methylhopane indices (MeHI) for bound C_{32}–C_{34} methylhopanes.

trace-metal fluxes increase with continental weathering is a topic that is relatively unexplored, but if we assume a roughly linear scaling, a doubling of the weathering Mo flux, holding all other parameters constant, would require a near doubling of seafloor area for a given environment (reducing or euxinic) to account for the same seawater Mo drawdown.

5.4. Trace metal limitation as a feedback on OAE duration and predictions for biotic response across different oceanographic settings

Upwelling at Site 1258 delivered significant amounts of ammonium, phosphorus, and other nutrients from the deep ocean (Higgins et al., 2012, and references therein), thereby supporting local primary production before, during and after OAE2 despite drawdown in bioessential trace elements during the event. Nonetheless, lipid biomarker analyses indicate substantial stratigraphic perturbations to the relative bacterial versus algal communities across OAE2 at Site 1258.

All of the H/St ratios are within the commonly observed Phanerozoic range for marine rocks (0.5–2.0), and eukaryotic organic contributions are appreciable. However, the stratigraphic trends in H/St values at this site are substantial, revealing systematic variation through the OAE (Fig. 5). Importantly, the observed increase in H/St during the OAE (up to 1.80) is driven by both an increase in hopanoid yields and a decrease in steroid biomarker yields, most likely arising from diminishing eukaryotic contributions to sedimentary organic matter during the OAE (Table S1), particularly during the peak of the OAE (Fig. 2). In other words, we see a systematic increase in the balance of bacterial to eukaryotic source inputs at Site 1258 during the OAE, likely reflecting their proportions in exported primary production. This increase is coincident with the decrease in trace metals and rebounds roughly synchronously with the observed trace metal trends—that is, subsequent to the OAE, local H/St ratios return to near pre-OAE values, generally coincident with recovery of trace metal enrichments.

The change in sterane number patterns observed (Fig. 5; see Section 4.2) suggests a shift away from chlorophyll c-containing biomarkers derived from red algal clades (haptophytes/diatoms)—which were abundant as marine plankton in the late Mesozoic and produced C_{28} steroids as major constituents—toward a eukaryotic primary producing community richer in rhodophyte and other red algal classes (including dinoflagellates) that produce C_{27} compounds as their major membrane sterols. The drop in the contribution of C_{28} steranes observed through OAE2 is in contrast to C_{28} sterane increases observed during oceanic anoxic events in the Paleozoic (Schwark and Empt, 2006), which we attribute to blooms of prasinophyte algae. These algae can better cope with nutrient stress compared with other green algae.

Analysis of HyPy products also reveals a series of C_{30} methylsteranes that includes 4-methylsteranes most commonly biosynthesized by dinoflagellate algae. A doubling in the abundance (from 2 to 4% of total kerogen-bound steranes) of four dinosterane diastereoisomers ($4\alpha,23,24$-trimethylcholestanes) and 4-methyl-24-ethylcholestane relative to regular (4-desmethyl) steranes is observed through OAE2 (Fig. 5) and provides direct evidence that dinoflagellates were important constituents of the planktonic community from red algal lineages that prospered during intervals marked by trace metal drawdown. This trend is consistent with previous studies that have indicated increased contribution of dinoflagellate cysts (van Helmond et al., 2014) and dinoflagellate biomarkers (Sepúlveda et al., 2009) through the positive carbon isotope excursion associated with OAE2. Importantly, dinoflagellates cope better than coccolithophorids under nitrogen and trace-metal stress (Erba, 2004), given their ability to form cysts and adapt to a mixotrophic lifestyle—that is, alternate between autotrophy and heterotrophy. As such, they have a competitive advantage over other eukaryotic phytoplankton during global drawdown of trace metals and fixed nitrogen, which also favored bacterial primary production. Dinosteranes are particularly abundant in other Mesozoic black shales deposited under euxinic marine conditions, such as the Jurassic Jet Rock and Kimmeridge Formations (e.g. Summons et al., 1992; Van Kaam-Peters and Sinninghe Damsté, 1997).

Although 2-methylhopanoids (2-MeHI) have a range of potential bacterial sources from cyanobacteria and proteobacteria (Welander et al., 2010), in the Cretaceous marine realm, N_2-fixing cyanobacteria remain a plausible source (Dumitrescu and Brassell, 2005; Kuypers et al., 2004b). Elevated 2-MeHI values (>5%) are associated with the onset of the C-isotope excursion and the highest H/St ratios measured in our samples (Fig. 5). The OAE proper reveals elevated 2-MeHI values of up to 22.5% (Table S2), which are significantly higher than those measured pre- and post-excursion.

Very high 2-MeHI values (>20%) have also been recorded in the aftermath of the end-Permian mass extinction in early Triassic strata from South China and are associated with a perturbation to the nitrogen cycle—apparently limited availability of nitrate—as evidenced by $\delta^{15}N_{org}$ reflecting a diazotrophic N_2-fixing bacterial signal (Cao et al., 2009).

Overall, a systematically diminishing relative eukaryotic contribution to sedimentary organic matter is observed at Site 1258 during the peak of OAE2, coincident with the lowest sedimentary Mo, V and Zn concentrations and hence the greatest oceanic drawdown. The biomarker ratios and abundance trends may most reasonably be interpreted to reflect an increase in the balance of bacterial to eukaryotic primary production during the OAE, which coincides locally with a drop in concentration of multiple transitional metals. At this point, the exact cause of this ecological perturbation is unclear but likely reflects one of the following or a combination: (1) Mo depletion that controlled fixed N assimilation by eukaryotes, (2) selection in favor of cyanobacteria under eutrophic conditions due to local upwelling of fixed N and/or, (3) essential metal limitation (such as Zn) for eukaryotes as a local factor. Furthermore, the structure of the eukaryotic planktonic community changed in composition to favor red algal lineages (such as rhodophytes and dinoflagellates) that coped best with the euxinic, nitrogen and trace metal stress observed during the peak of OAE2. Locally site 1258 maintained high levels of organic carbon burial despite possible metal limitation during the OAE due to high local nutrient availability from upwelling of nutrient-rich waters reducing the local impact of nitrogen-stress on eukaryotes such as microalgae (Higgins et al., 2012).

6. Summary and conclusions

The observed stratigraphic trends in redox sensitive trace metals, when combined with the global record of low Mo/TOC and geochemical modeling of the marine Mo inventory, suggest that the globally integrated ocean could have had Mo concentrations on the order of those expected to impact biological metabolism (Glass et al., 2010; Zerkle et al., 2006). Importantly, ocean-scale euxinia is not required, less than 7% seafloor area is sufficient, for the drawdown of redox sensitive trace metals. The observed patterns can instead be explained by highly productive continental margin settings. Locally, Site 1258 maintained high levels of organic carbon burial, despite possible metal limitation during the OAE, due to upwelling of fixed nitrogen. For areas along continental margins but outside of upwelling regions, we suggest that oxygen-limitation and associated microbial loss of fixed nitrogen was compounded by limitations in bioessential trace metals. These metals are required for cyanobacterial enzymes to replenish the fixed nitrogen pool and sustain marine productivity—specifically within less intense upwelling regions along continental margins and within central portions of the ocean. Ultimately, the observed trace metal drawdown during OAE2 may have been an important biological feedback mechanism that eventually limited the duration of this massive carbon burial event during the well oxygenated Mesozoic.

Site 1258 was locally euxinic throughout the analyzed section, but the observed decline in V enrichment predates the carbon isotope excursion and the Mo drawdown. This observation suggests a global expansion of low-oxygen/anoxic conditions without appreciable sulfide accumulation in the water column prior to initiation of OAE2, which is consistent with the idea of widespread oxygen deficiency. Interestingly, this pre-event decline in marine oxygen roughly correlates with increased turnover rates for radiolarians (Leckie et al., 2002, and references therein). Of equal significance, the predicted expansion of seafloor euxinia and other reducing settings at the onset of OAE2, as defined by Mo, correlates broadly with increased turnover rates for calcareous nannofossils and benthic and planktonic foraminifera (Leckie et al., 2002). Fig. 6 presents an overview of current understanding of these global relationships. Additionally, the low spatial and, in some cases, temporally variable extent of a toxic euxinic ocean may help explain some of the limited extinction patterns observed in some clades (i.e., large portions of the ocean remain oxygenated). For example, it has been suggested that some of the epeiric seaway sites became more ventilated during the OAE based on increased bioturbation and a decrease in trace element enrichments (Eldrett et al., 2014; Meyers et al., 2005, 2012). However, muted trace element enrichments could also reflect the decreased marine inventory that we describe in this paper.

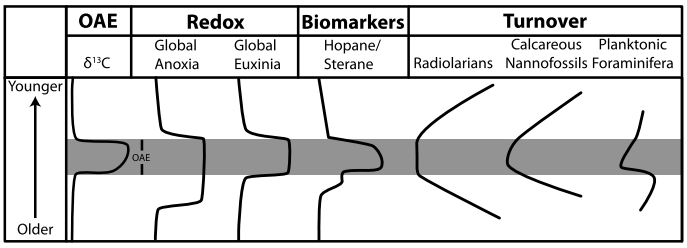

Fig. 6. Generalized relative stratigraphic changes of carbon isotopes (as reviewed in Jenkyns, 2010), redox conditions (from this study, Hetzel et al., 2009, Owens et al., 2012, 2013) and biomarker data (this study) and turnover rates (speciation and extinction) for three marine plaktonic protists (Leckie et al., 2002) during OAE2.

The observed positive carbon-isotope excursion demands increased global carbon burial throughout OAE2 even in the face of decreasing essential micronutrient supply. Our favored hypothesis is that increased productivity initiated the event, caused by a pulse of nutrient delivery from either greater hydrothermal fluxes, climatically induced accelerated weathering or other factors acting alone or in combination. Then, enhanced preservation of organic matter under conditions of low oxygen and high sedimentation became the dominant controls—particularly in marginal settings such as epeiric seaways and coastal upwelling zones. The organic carbon burial that drove the positive C excursion may have been associated with enhanced preservation in productive euxinic hotspots—consistent with past estimates of 3 to 7% for the areal extent of euxinia (Owens et al., 2013).

Global expansion of low oxygen marine conditions in the Phanerozoic ocean are often manifest as short-lived, discrete events (<1 million yrs), perhaps at least in part as a result of biological metal feedbacks. Ultimately, the generally more reducing OAE ocean favored decreased supplies of fixed nitrogen and related inventories of bio-essential trace metals needed to sustain high productivity. These factors, along with copious oxygen release and subsequent cooling from atmospheric drawdown of CO_2 through the global burial of organic carbon (as reviewed in Jenkyns, 2010), would have acted as negative feedbacks that returned the ocean to more generally oxidizing conditions. A similar chain of events may have played out repeatedly in the history of marine anoxia.

Acknowledgements

B. Gill and N. Planavsky provided insight during the early stages of this project. The samples were obtained through Walter Hale at the Bremen IODP Core Repository. This manuscript has benefited from reviews by Chris Junium, Mark Leckie, an anonymous reviewer and editorial direction from Derek Vance. We thank Mark Williams and Carina Lee for help with organic biomarker laboratory analyses. TWL, GDL, JDO and CTR thank the NASA Astrobiology Institute (NNA15BB03A), the NSF (EAR-1338299 [ELT Program] and OCE-1624895) and the Agouron Institute for financial support.

Appendix A. Supplementary material

Supplementary material related to this article can be found online at http://dx.doi.org/10.1016/j.epsl.2016.05.046.

References

Algeo, T.J., 2004. Can marine anoxic events draw down the trace element inventory of seawater? Geology 32, 1057–1060.

Algeo, T.J., Lyons, T.W., 2006. Mo – total organic carbon covariation in modern anoxic marine environments: implications for analysis of paleoredox and paleohydrographic conditions. Paleoceanography 21, PA1016.

Algeo, T.J., Rowe, H., 2011. Paleoceanographic applications of trace-metal concentration data. Chem. Geol. 324–325, 6–18.

Bambach, R.K., 2006. Phanerozoic biodiversity mass extinctions. Annu. Rev. Earth Planet. Sci. 34, 127–155.

Bellenger, J.P., Wichard, T., Xu, Y., Kraepiel, A.M.L., 2011. Essential metals for nitrogen fixation in a free-living N_2-fixing bacterium: chelation, homeostasis and high use efficiency. Environ. Microbiol. 13, 1395–1411.

Berner, R.A., Beerling, D.J., Dudley, R., Robinson, J.M., Wildman, R.A., 2003. Phanerozoic atmospheric oxygen. Annu. Rev. Earth Planet. Sci. 31, 105–134.

Blumenberg, M., Wiese, F., 2012. Imbalanced nutrients as triggers for black shale formation in a shallow shelf setting during the OAE 2 (Wunstorf, Germany). Biogeosci. Discuss. 9, 4139–4153.

Böttcher, M.E., Hetzel, A., Brumsack, H.J., Schipper, A., 2006. Sulfur–iron–carbon geochemistry in sediments of the Demerara Rise. In: Mosher, D.C., Erbacher, J., Malone, M.J. (Eds.), Proceedings of the Ocean Drilling Program Scientific Results, vol. 207. Ocean Drilling Program, College Station, TX, pp. 1–23.

Canfield, D.E., Raiswell, R., Westrich, J.T., Reaves, C.M., Berner, R.A., 1986. The use of chromium reduction in the analysis of reduced inorganic sulfur in sediments and shales. Chem. Geol. 54, 149–155.

Cao, C., Love, G.D., Hays, L.E., Wang, W., Shen, S., Summons, R.E., 2009. Biogeochemical evidence for euxinic oceans and ecological disturbance presaging the end-Permian mass extinction event. Earth Planet. Sci. Lett. 281, 188–201.

Dickson, A.J., Jenkyns, H.C., Porcelli, D., van den Boorn, S., Idiz, E., 2016. Basin-scale controls on the molybdenum-isotope composition of seawater during Oceanic Anoxic Event 2 (Late Cretaceous). Geochim. Cosmochim. Acta 178, 291–306.

Dumitrescu, M., Brassell, S.C., 2005. Biogeochemical assessment of sources of organic matter and paleoproductivity during the early Aptian Oceanic Anoxic Event at Shatsky Rise, ODP Leg 198. Org. Geochem. 36, 1002–1022.

Eldrett, J.S., Minisini, D., Bergman, S.C., 2014. Decoupling of the carbon cycle during Ocean Anoxic Event 2. Geology 42 (7), 567–570.

Erba, E., 2004. Calcareous nannofossils and Mesozoic oceanic anoxic events. Mar. Micropaleontol. 52, 85–106.

Erbacher, J., Mosher, D.C., Malone, M.J., et al., 2004. Proc. ODP. Init. Repts. 207. Ocean Drilling Program, College Station, TX, pp. 1–89.

Erbacher, J., Friedrich, O., Wilson, P.A., Birch, H., Mutterlose, J., 2005. Stable organic carbon isotope stratigraphy across Oceanic Anoxic Event 2 of Demerara Rise, western tropical Atlantic. Geochem. Geophys. Geosyst. 6, Q06010.

Forster, A., Sturt, H., Meyers, P.A., 2004. Molecular biogeochemistry of Cretaceous black shales from the Demerara Rise: preliminary shipboard results from Sites 1257 and 1258. Proceedings of the Ocean Drilling Program, Initial Reports 207.

Forster, A., et al., 2008. The Cenomanian/Turonian oceanic anoxic event in the South Atlantic: new insights from a geochemical study of DSDP Site 530A. Palaeogeogr. Palaeoclimatol. Palaeoecol. 267 (3–4), 256–283.

Giner, J.-L., Zhao, H., Boyer, G.L., Satchwell, M.F., Andersen, R.A., 2009. Sterol chemotaxonomy of marine pelagophyte algae. Chem. Biodivers. 6, 1111–1130.

Glass, J.B., Wolfe-Simon, F., Elser, J.J., Anbar, A.D., 2010. Molybdenum-nitrogen co-limitation in freshwater and coastal heterocystous cyanobacteria. Limnol. Oceanogr. 55, 667–676.

Goldberg, T., Poulton, S.W., Wagner, T., Kolonic, S.F., Rehkämper, M., 2016. Molybdenum drawdown during Cretaceous Oceanic Anoxic Event 2. Earth Planet. Sci. Lett. 440, 81–91.

Grabenstatter, J., Méhay, S., McIntyre-Wressnig, A., Giner, J.-L., Edgcomb, V.P., Beaudoin, D.J., Bernhard, J.M., Summons, R.E., 2013. Identification of 24-n-propylidenecholesterol in a member of the Foraminifera. Org. Geochem. 63, 145–151.

Grantham, P.J., Wakefield, L.L., 1988. Variations in the sterane carbon number distributions of marine source rock derived crude oils through geological time. Org. Geochem. 12, 61–73.

Hetzel, A., Böttcher, M.E., Wortmann, U.G., Brumsack, H.-J., 2009. Paleo-redox conditions during OAE 2 reflected in Demerara Rise sediment geochemistry (ODP Leg 207). Palaeogeogr. Palaeoclimatol. Palaeoecol. 273 (3–4), 302–328.

Hetzel, A., März, C., Vogt, C., Brumsack, H.-J., 2011. Geochemical environment of Cenomanian–Turonian black shale deposition at Wunstorf (northern Germany). Cretac. Res. 32, 480–494.

Higgins, M.B., Robinson, R.S., Husson, J.M., Carter, S.J., Pearson, A., 2012. Dominant eukaryotic export production during ocean anoxic events reflects the importance of recycled NH_4^+. Proc. Natl. Acad. Sci. 109, 2269–2274.

Jenkyns, H.C., 2010. Geochemistry of oceanic anoxic events. Geochem. Geophys. Geosyst. 11, Q03004.

Junium, C.K., Freeman, K.H., Arthur, M.A., 2015. Controls on the stratigraphic distribution and nitrogen isotopic composition of zinc, vanadyl and free base porphyrins through Oceanic Anoxic Event 2 at Demerara Rise. Org. Geochem. 80, 60–71.

Kodner, R.B., Summons, R.E., Pearson, A., King, N., Knoll, A.H., 2008. Sterols in a unicellular relative of the metazoans. Proc. Natl. Acad. Sci. 105, 9897–9902.

Kohnen, M.E.L., Schouten, S., Sinninghe Damsté, J.S., de Leeuw, J.W., Merrit, D., Hayes, J.M., 1992. The combined application of organic sulphur and isotope geochemistry to asses multiple sources of palaeobiochemicals with identical carbon skeletons. Org. Geochem. 19, 403–419.

Kraal, P., Slomp, C.P., Forster, A., Kuypers, M.M.M., 2010. Phosphorus cycling from the margin to abyssal depths in the proto-Atlantic during oceanic anoxic event 2. Palaeogeogr. Palaeoclimatol. Palaeoecol. 295, 42–54.

Kuypers, M.M.M., Lourens, L.J., Rijpstra, W.I.C., Pancost, R.D., Nijenhuis, I.A., Sinninghe Damsté, J.S., 2004a. Orbital forcing of organic carbon burial in the proto-North Atlantic during oceanic anoxic event 2. Earth Planet. Sci. Lett. 228, 465–482.

Kuypers, M.M.M., van Breugel, Y., Schouten, S., Erba, E., Damsté, J.S.S., 2004b. N_2-fixing cyanobacteria supplied nutrient N for Cretaceous oceanic anoxic events. Geology 32 (10), 853–856.

Leckie, R.M., Bralower, T.J., Cashman, R., 2002. Oceanic anoxic events and plankton evolution: biotic response to tectonic forcing during the mid-Cretaceous. Paleoceanography 17, PA000623.

Lenniger, M., Nøhr-Hansen, H., Hills, L.V., Bjerrum, C.J., 2014. Arctic black shale formation during Cretaceous Oceanic Anoxic Event 2. Geology 42 (9), 799–802.

Little, S.H., Vance, D., Walker-Brown, C., Landing, W.M., 2014. The oceanic mass balance of copper and zinc isotopes, investigated by analysis of their inputs, and outputs to ferromanganese oxide sediments. Geochim. Cosmochim. Acta 125, 673–693.

Little, S.H., Vance, D., Lyons, T.W., McManus, J., 2015. Controls on trace metal authigenic enrichment in reducing sediments: insights from modern oxygen-deficient settings. Am. J. Sci. 315, 77–119.

Love, G.D., Snape, C.E., Carr, A.D., Houghton, R.C., 1995. Release of covalently-bound alkane biomarkers in high yields from kerogen via catalytic hydropyrolysis. Org. Geochem. 23, 981–986.

Lu, Z., Jenkyns, H.C., Rickaby, R.E.M., 2010. Iodine to calcium ratios in marine carbonate as a paleo-redox proxy during oceanic anoxic events. Geology 38, 1107–1110.

Lyons, T.W., Anbar, A.D., Severmann, S., Scott, C., Gill, B.C., 2009. Tracking Euxinia in the Ancient Ocean: a multiproxy perspective and proterozoic case study. Annu. Rev. Earth Planet. Sci. 37, 507–534.

Lyons, T.W., Reinhard, C.T., Planavsky, N.J., 2014. The rise of oxygen in Earth's early ocean and atmosphere. Nature 506 (7488), 307–315.

MacLeod, K.G., Martin, E.E., Blair, S.W., 2008. Nd isotopic excursion across Cretaceous ocean anoxic event 2 (Cenomanian–Turonian) in the tropical North Atlantic. Geology 36, 811–814.

März, C., Poulton, S.W., Beckmann, B., Küster, K., Wagner, T., Kasten, S., 2008. Redox sensitivity of P cycling during marine black shale formation: dynamics of sulfidic and anoxic, non-sulfidic bottom waters. Geochim. Cosmochim. Acta 72, 3703–3717.

Meyers, S.R., Sageman, B.B., Lyons, T.W., 2005. Organic carbon burial rate and the molybdenum proxy: theoretical framework and application to Cenomanian–Turonian oceanic anoxic event 2. Paleoceanography 20, PA2002.

Meyers, S.R., Sageman, B.B., Arthur, M.A., 2012. Obliquity forcing of organic matter accumulation during Oceanic Anoxic Event 2. Paleoceanography 27.

Miller, C.A., Peucker-Ehrenbrink, B., Walker, B.D., Marcantonio, F., 2011. Re-assessing the surface cycling of molybdenum and rhenium. Geochim. Cosmochim. Acta 75, 7146–7179.

Monteiro, F.M., Pancost, R.D., Ridgwell, A., Donnadieu, Y., 2012. Nutrients as the dominant control on the spread of anoxia and euxinia across the Cenomanian–Turonian oceanic anoxic event (OAE2): model-data comparison. Paleoceanography 27, PA4209.

Morford, J.L., Emerson, S., 1999. The geochemistry of redox sensitive trace metals in sediments. Geochim. Cosmochim. Acta 63, 1735–1750.

Owens, J.D., Lyons, T.W., Li, X., Macleod, K.G., Gordon, G., Kuypers, M.M.M., Anbar, A., Kuhnt, W., Severmann, S., 2012. Iron isotope and trace metal records of iron cycling in the proto-North Atlantic during the Cenomanian–Turonian oceanic anoxic event (OAE-2). Paleoceanography 27, PA3223.

Owens, J.D., Gill, B.C., Jenkyns, H.C., Bates, S.M., Severmann, S., Kuypers, M.M.M., Woodfine, R.G., Lyons, T.W., 2013. Sulfur isotopes track the global extent and dynamics of euxinia during Cretaceous Oceanic Anoxic Event 2. Proc. Natl. Acad. Sci. 110, 18407–18412.

Pogge von Strandmann, P.A.E., Jenkyns, H.C., Woodfine, R.G., 2013. Lithium isotope evidence for enhanced weathering during Oceanic Anoxic Event 2. Nat. Geosci. 6, 668–672.

Poulton, S., Canfield, D., 2005. Development of a sequential extraction procedure for iron: implications for iron partitioning in continentally-derived particulates.

Chem. Geol. 214, 209–221.
Poulton, S.W., Canfield, D.E., 2009. Ferruginous conditions: a dominant feature of the ocean through Earth's history. Elements 7, 107–112.
Raiswell, R., Berner, R.A., 1986. Pyrite and organic matter in Phanerozoic normal marine shales. Geochim. Cosmochim. Acta 50, 1967–1976.
Reinhard, C.T., Planavsky, N.J., Robbins, L.J., Partin, C.A., Gill, B.C., Lalonde, S.V., Bekker, A., Konhauser, K.O., Lyons, T.W., 2013. Proterozoic ocean redox and biogeochemical stasis. Proc. Natl. Acad. Sci. 110, 5357–5362.
Schwark, L., Empt, P., 2006. Sterane biomarkers as indicators of palaeozoic algal evolution and extinction events. Palaeogeogr. Palaeoclimatol. Palaeoecol. 240, 225–236.
Scotese, C.R., 2008. The PALEOMAP Project PaleoAtlas for ArcGIS, Volume 2. Cretaceous Paleogeographic and Plate Rectonic Reconstructions. PALEOMAP Project.
Scott, C., Lyons, T.W., 2012. Contrasting molybdenum cycling and isotopic properties in euxinic versus non-euxinic sediments and sedimentary rocks: refining the paleoproxies. Chem. Geol. 324–325, 19–27.
Sepúlveda, J., Wendler, J., Leider, A., Kuss, H.-J., Summons, R.E., Hinrichs, K.-U., 2009. Molecular isotopic evidence of environmental and ecological changes across the Cenomanian–Turonian boundary in the Levant Platform of central Jordan. Org. Geochem. 40, 553–568.
Sinninghe Damsté, J.S., de Leeuw, J.W., 1990. Analysis, structure and geochemical significance of organically-bound sulphur in the geosphere: state of the art and future research. Org. Geochem. 16, 1077–1101.
Summons, R.E., Thomas, J., Maxwell, J.R., Boreham, C.J., 1992. Secular and environmental constraints on the occurrence of dinosterane in sediments. Geochim. Cosmochim. Acta 56, 2437–2444.
Taylor, S.R., McLennan, S.M., 1995. The geochemical evolution of the continental crust. Rev. Geophys. 33, 241–265.
Tribovillard, N., Algeo, T.J., Lyons, T., Riboulleau, A., 2006. Trace metals as paleoredox and paleoproductivity proxies: an update. Chem. Geol. 232, 12–32.
Turgeon, S., Brumsack, H.-J., 2006. Anoxic vs dysoxic events reflected in sediment geochemistry during the Cenomanian–Turonian Boundary Event (Cretaceous) in the Umbria-Marche Basin of central Italy. Chem. Geol. 234, 321–339.
van Helmond, N.A.G.M., Sluijs, A., Reichart, G.-J., Sinninghe Damsté, J.S., Slomp, C.P., Brinkhuis, H., 2014. A perturbed hydrological cycle during Oceanic Anoxic Event 2. Geology 42, 123–126.
Van Kaam-Peters, H.M.E., Sinninghe Damsté, J.S., 1997. Characterisation of an extremely organic sulphur-rich, 150 Ma old carbonaceous rock: palaeoenvironmental implications. Org. Geochem. 27, 371–397.
Voigt, S., Erbacher, J., Mutterlose, J., Weiss, W., Westerhold, T., Wiese, F., Wilmsen, M., Wonik, T., 2008. The Cenomanian–Turonian of the Wunstorf section – (North Germany): global stratigraphic reference section and new orbital time scale for Oceanic Anoxic Event 2. Newsl. Stratigr. 43, 65–89.
Volkman, J., 2003. Sterols in microorganisms. Appl. Microbiol. Biotechnol. 60, 495–506.
Welander, P.V., Coleman, M.L., Sessions, A.L., Summons, R.E., Newman, D.K., 2010. Identification of a methylase required for 2-methylhopanoid production and implications for the interpretation of sedimentary hopanes. Proc. Natl. Acad. Sci. 107, 8537–8542.
West, A.J., Galy, A., Bickle, M., 2005. Tectonic and climatic controls on silicate weathering. Earth Planet. Sci. Lett. 235, 211–228.
Westermann, S., Vance, D., Cameron, V., Archer, C., Robinson, S.A., 2014. Heterogeneous oxygenation states in the Atlantic and Tethys oceans during Oceanic Anoxic Event 2. Earth Planet. Sci. Lett. 404, 178–189.
Zerkle, A.L., House, C.H., Cox, R.P., Canfield, D.E., 2006. Metal limitation of cyanobacterial N_2 fixation and implications for the Precambrian nitrogen cycle. Geobiology 4, 285–297.
Zhang, X., Sigman, D.M., Morel, F.M.M., Kraepiel, A.M.L., 2014. Nitrogen isotope fractionation by alternative nitrogenases and past ocean anoxia. Proc. Natl. Acad. Sci. 111, 4782–4787.